Fizika Nizkikh Temperatur, 2003, v. 29, Nos. 9/10, p. 1113–1117

Luminescence and formation of alkalihalide ionic excimers in solid Ne and Ar

G. Śliwiński and M. Frankowski

Polish Academy of Sciences, IF-FM, Fiszera 14, PL 80-952 Gdansk, Poland
E-mail: gerards@imp.gda.pl

N. Schwentner

Institute of Experimental Physics, Free University, Arnimallee 14, Berlin D-14195, Germany

Transitions from ionic states $A^{2+}X^-$ of alkalihalides CsF, CsCl and RbF isolated in solid Ne and Ar films recorded under pulsed *e*-beam excitation are studied. The $B(^2\Sigma_{1/2})$–$X(^2\Sigma_{1/2})$ and $C(^2\Pi_{3/2})$–$A(^2\Pi_{3/2})$ luminescence bands of $Cs^{2+}F^-$ (196.5 nm, 227 nm), $Cs^{2+}Cl^-$ (220.1 nm, 249.2 nm) and $Rb^{2+}F^-$ (136 nm) in Ne, and a weaker B–X emission of $Cs^{2+}F^-$ (211.2 nm) in Ar are identified. For CsF the depopulation of the $A^{2+}X^-$ state is dominated by the radiative decay. A ratio of the recorded exciplex emission intensities of $I(\mathrm{CsF})/I(\mathrm{CsCl})/I(\mathrm{RbF}) = 20/5/1$ reflects the luminescence efficiency and for RbF and CsCl a competitive emission channel due to predissociation in the $A^{2+}X^-(B^2\Sigma_{1/2})$ state is observed. For these molecules an efficient formation of the state X_2^* is confirmed through recording the molecular $D'(^3\Pi_{2g})$–$A'(^3\Pi_{2u})$ transition. A strong dependence of the luminescence intensities on the alkalihalide content reveals quenching at concentrations higher than 0.7%.

PACS: **78.45.+h**, 78.55.Fv

1. Introduction

Luminescence of ionic excimers covers the VUV and deep UV wavelength region and represents an interesting perspective for an extension of the gas phase excimer media towards shorter wavelengths. Since the first considerations around 1985 [1,2] the ionic systems are extensively investigated. Spectroscopic studies in the gas phase provided emission from ionic states $A^{2+}X^-$ of alkalihalides (AX), and from diatomic $(RgA)^+$ and triatomic $(Rg_2A)^+$ rare gas alkali ions [3–8]. Optical gain has been achieved [9], however, the recent kinetic studies indicate quenching processes which can seriously limit amplification [10].

The electronic configurations for the family of alkalihalide ions $(AX)^+$ correspond to those of rare gas halides RgX in the ground state and correlate to the atomic states $A^+(^1S)$ and $X(^2P)$. Also the ionically bound upper states $(A^{2+}X^-)$ due to transfer of an alkali 5*p*-core electron to the halogen are isoelectronic to Rg^+X^- exciplex states with similar potential surfaces and correlate to $A^{2+}(^2P)$ and $X^-(^1S)$ atomic states. Since the potential of the lower $(AX)^+$ state has a dissociative character it is anticipated, that population inversion can be obtained in these systems. The upper bound state can be directly populated by photoionization of AX. Radiative transitions with large cross-section for stimulated emission and short radiative lifetimes of the order of 1 ns can be expected for $A^{2+}X^-$. These ions considered in the condensed phase combine the favorable properties of the short wavelength, strong excimer emissions known from the gas phase with the high number densities of excited states attainable in the solid.

Recently deep UV fluorescence bands of $A^{2+}X^-$ ions were observed for CsF, CsCl and RbF isolated in Ne and Ar matrices under *e*-beam excitation [11,12]. It was shown, that the exciplex states $B^2\Sigma_{1/2}$ and $X^2\Pi_{3/2}$ are effectively populated via host excitons resulting mainly in the $B^2\Sigma_{1/2} \rightarrow X^2\Sigma_{1/2}$ emission. Also a much weaker $C^2\Pi_{3/2} \rightarrow A^2\Pi_{3/2}$ transition for the ionic states of CsF and CsCl was observed. The observed transitions were red shifted compared to the gas phase due to interaction with the dielectric host. The first indication for the homonuclear D'–A' transition of Cl_2^* and F_2^* was reported and ascribed to predissociation via the A^+X^* state [13].

In this work the spectroscopic data and formation of the ionic states $A^{2+}X^-$ of alkalihalides: CsF, CsCl and RbF isolated in thin Ne and Ar films, are studied. Conclusions on the formation efficiency of X_2^* molecules due to predissociation in the $A^{2+}X^-(B^2\Sigma_{1/2})$ state of RbF and CsCl following from the concentration dependent measurements are discussed.

2. Transitions from alkalihalide ionic states

For understanding of the excitation and decay processes it is instructive to consider the energy level scheme of the alkalihalide states involved in the observed radiative transitions. Since the problem was discussed for the CsCl elsewhere [12] here just features will be recalled which are valid for the general case of the A^+X^- ionic states. For this purpose it is convenient to consider the energy of states in units equal to the binding potential of the AX ground state and the internuclear separation in units of equilibrium distance r_e – see Fig. 1. The states relevant for discussion are described by potential curves and for the other ones only

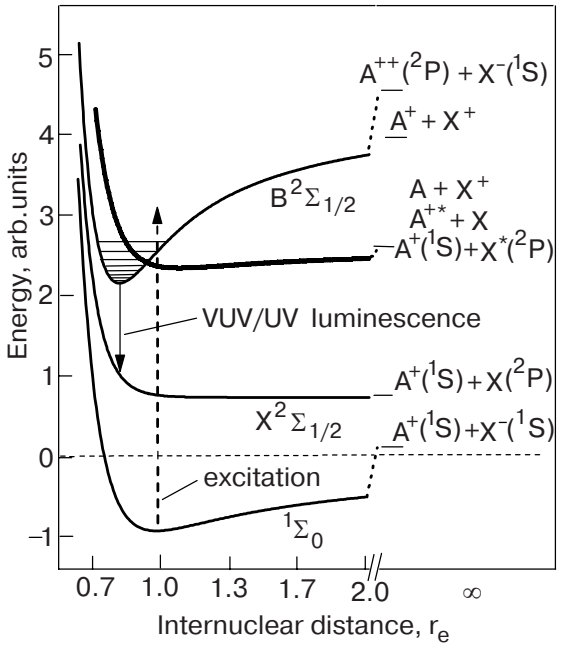

Fig. 1. The potential energy diagram of the alkalihalides; energy and internuclear separation are in units of the ground state binding potential, and r_e, respectively; the relevant states are described by the shell configurations and for the other ones only the energetic positions at $r = \infty$ are given; states $C^2\Pi$ and $A^2\Pi$ resulting from the spin-orbit splitting of the upper and lower excimer state, respectively, are not shown for simplicity. Selective excitation of the ground state A^+X^- molecule is provided by the e-beam via rare gas excitons — dashed arrow. The radiative decay follows a fast radiationless relaxation to the $\nu' = 0$ level of the $A^{2+}X^-$ ionic bound state.

positions of the dissociation limits are given. The rare gas excitons formed in the host by the pulsed electron beam are responsible for the $A^+(^1S)$ core ionization of the $^1\Sigma$ ground state of AX molecules (an upward arrow in Fig. 1). Due to the equilibrium distance r_e in this state the higher vibrational levels ν'' of the $A^{2+}(^2P)X^-(^1S)$ state are populated, and a fast radiationless relaxation to the $\nu'' = 0$ level occurs because of the low temperature around 5 K. It is followed by the bound-free radiative transition

$$A^{2+}X^- \Rightarrow (AX)^+ + h\nu \qquad (1)$$

to the repulsive part of the lower $X^2\Sigma_{1/2}$ potential and characterized by the emission of UV photons on a time scale close to one nanosecond (a downward arrow, Fig. 1). Energy wise population of the closely spaced B and C states of $A^{2+}X^-$ is equally likely and emissions from these states are observed in contrary to the D state which lies higher in energy by the $^2P_{3/2} - ^2P_{1/2}$ spin-orbit splitting of the A^{2+} ion.

The bound states, i.e. the ground state $^1\Sigma$, the A^+X^*, and the ionic $B^2\Sigma_{1/2}$, potential curves in Fig. 1 are based on the truncated Rittner potential (at $1/r^4$) with the effect of the dielectric host taken into account by introducing the $1/\varepsilon$ factor into the coulombic and $1/r^4$ terms. Bond lengths and polarizabilities are taken from literature [4,14]. For the lower A^+X state the Born–Mayer potential

$$V(r) = \varepsilon_0 \exp[-\alpha_0 (r - r_e)] \qquad (2)$$

is used with the assumption that the consideration refers to the vicinity of the equilibrium distance r_e, with ε_0 being the energy of the lower state at $r = r_e$. The shape of $V(r)$ and also the ε_0 and α_0 values are derived from experimental data for the gas phase B–X transitions of $A^{2+}X^-$ ions. The potential minima of the $X^2\Sigma_{1/2}$ states are taken equal to their gas phase counterparts [4].

The transition energies observed in experiment are red shifted by ΔE relative to the gas phase. This can be explained by means of the cavity shell model for a transition dipole moment $\Delta|\mu|$ given by the relation

$$(\Delta|\mu|)^2 = C(\varepsilon)\Delta E d^3 \qquad (3)$$

with $C(\varepsilon) = 0.125(2\varepsilon + 1)/(\varepsilon - 1)$, d corresponding to the cavity diameter, and ε being the dielectric constant of the surrounding. The measured ΔE values yield the estimates for $\Delta|\mu|$ and the measured transition energies result in potential minima of the upper $A^{2+}X^-(B^2\Sigma_{1/2})$ states with the red shifts reflecting the solvation energy of the ionic states of AX molecules.

For CsCl and RbF it can be deduced from Fig. 1, that the Frank—Condon region corresponding to the

excitation of the $^1\Sigma$ state falls close to the crossing point of the $A^{2+}X^-$ and A^+X^* potential surfaces. This indicates predissociation of the $A^{2+}X^-$ state as the probable depopulation channel due to the reaction

$$A^{2+}X^- \Rightarrow A^+ + X^* \qquad (4)$$

which is accompanied by a partial, nonradiative energy loss. Similar to the gas phase results [5] the competing predissociation effect is only observed for CsCl and RbF doped samples and in both cases the X_2^* molecular emission

$$X_2^* \Rightarrow X_2 + h\nu_1, \quad h\nu_1 < h\nu \qquad (5)$$

occurs. However, in the host a strong cage effect traps the excited X^* atoms in the lattice. This leads to a decrease of the population of X_2 molecules finally formed in the ground state. For CsF doped samples the X_2^* emission was not observed so in the matrix as well as in the gas phase. The difference in separations of the crossing point of $A^{2+}X^-$ and A^+X^* potentials from the bottom of the $^1\Sigma$ potential ($r_e = 1$) in Fig. 1, and also the longer radiative lifetime of the *C* state explain the low intensity of the *C*–*A* band for CsF and CsCl in Ne obtained from experiment. The spectroscopic data of the observed ionic transitions for RbF, CsCl, and CsF are calculated following the procedure described previously [15], and are given in Table.

Table

Spectroscopic properties of matrix isolated, core excited RbF, CsF and CsCl alkalihalides in the VUV and deep UV spectral range: λ_{em} — peak position, fwhm — halfwidth, σ_s — cross section for stimulated emission, and τ_f — radiative lifetime

Molecule, transition	Matrix	λ_{em}, nm	fwhm, nm	σ_s, 10^{-16} cm^2	τ_r, ns
$Rb^{++}F^-$					
$B \to X$	Ne	136	4.5	1.5	0.9
$Cs^{++}F^-$					
$B \to X$	Ne	196.5	9.5	2.5	1.2
$C \to A$	Ne	227.1	15	0.22	11.3
$B \to X$	Ar	211.2	11.3	2.74	0.8
$Cs^{++}Cl^-$					
$B \to X$	Ne	220.1	10.4	2.22	1.4
$C \to A$	Ne	249.2	14.8	0.29	12.6

As the most of data obtained refer to the Ne host a comment should be added for the transition energies observed in the solid. These are shown as the matrix-dependent (Ne, Ar, or Kr) peak positions of the emission bands together with respective data from gas phase measurements and those of the solid state XeF excimer for reference – Fig. 2. The peak positions are given for optimal contents of the alkalihalides CsF (0.45% in Ar, and 0.7% in Ne), CsCl (0.37%), and RbF (0.6%) in solid Ar and Ne films. The variable $(\varepsilon - 1)/(2\varepsilon + 1)$ describes the host interaction and slanted lines connect data of the same dopant. In comparison to the gas phase results [5] the matrix shift of the $B \to X$ luminescence from the ionic states of RbF, CsF and CsCl has a value of 0.43, 0.39 and 0.33 eV, respectively. This is in a good agreement with values of 0.3–0.4 eV predicted from relation (3) and coincides with the results obtained for the XeF excimer in solid Ne and Ar [15,16]. Moreover, the values obtained so far from experiment (solid data points) allow to deduce the estimates of transition energies for

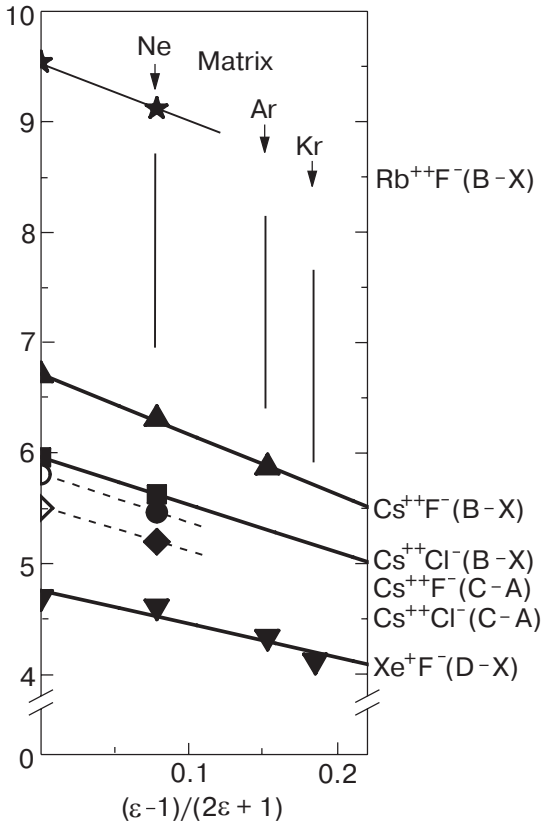

Fig. 2. The matrix-dependent transition energies of the *e*-beam excited CsF, CsCl, and RbF in Ar and Ne solid films for the optimal alkalihalide concentrations, and XeF data for reference; values for $(\varepsilon - 1)/(2\varepsilon + 1) = 0$ correspond to the gas phase data already measured (solid data points) and postulated (hollow points).

emission bands not observed yet in the solid and in the gas phase as well (hollow data points).

3. The concentration effect

The measured intensities of the B–X band are highly sensitive to changes in the original sample composition. Dependences of the peak intensity values versus the dopant concentrations in Ne films presented in the form of experimental data sets for CsF, RbF (up and down triangles), and CsCl (squares) are summarized in Fig. 3. The dependence observed for CsCl is more pronounced than for CsF and for RbF only two data points are available due to the relatively low signal. In all cases the optimal alkalihalide content corresponding to the maximum band intensity lies around 0.6–0.8% and is in accordance with the data obtained for the gas phase [4] and also coincides with those from our previous results reported for XeF [15,16]. A comparison of the band intensities for the optimal concentrations related to the highest one (CsF) lead to the ratio of $I(\mathrm{CsF})/I(\mathrm{CsCl})/I(\mathrm{RbF}) = 20/5/1$ and reflects the energy transfer efficiency for the investigated species. In the case of CsF a change of the concentration dependent intensity of almost two orders of magnitude is observed.

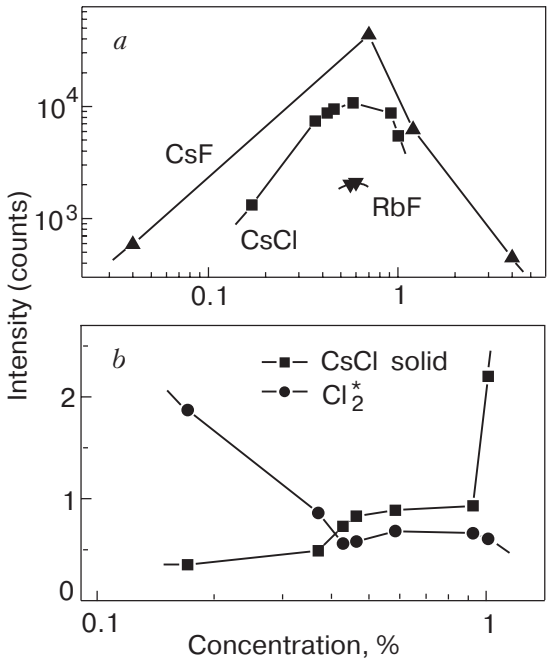

Fig. 3. Emission intensities of the $B \to X$ transition of the $A^{2+}X^-$ exciplexes vs. the AX concentration in Ne solid films for CsF (▲), CsCl (■) and for RbF (▼) (*a*), and the case of CsCl doped Ne sample; luminescence intensities of the Cl_2^* molecular transition $D'(^3\Pi_{2g}) \to A'(^3\Pi_{2u})$ and of the intrinsic band of CsCl aggregates (245 nm), related to the $B^2\Sigma_{1/2} \to X^2\Sigma_{1/2}$ band intensity vs. concentration (*b*); concentrations are percentages and intensities are the peak values measured.

The data for CsCl indicate on weaker concentration dependence for samples doped below optimum than for the higher doped ones. In the low doping range exclusively an occurrence of the predissociation of molecules in the ionic state can be observed. This is confirmed by the detailed analysis of the CsF and CsCl spectra reported elsewhere [11,12]. The relevant decay channels of the $Cs^{2+}Cl^-(B^2\Sigma_{1/2})$ state become more evident when the $D'(^3\Pi_{2g}) \to A'(^3\Pi_{2u})$ transition of the Cl_2^* molecule is taken into account. An appearance of the molecular emission can only be observed for CsCl content not exceeding values of about 0.6–0.7%. The intensity of this transition is even much larger from that of B–X for lower concentrations, around 0.1–0.2 %. This together with a decrease of the Cl_2^* band intensity for CsCl content increasing in that range reflects a strong competition between the deep UV emission and the concentration quenching process which is due to short-range energy migration, aggregation and also self-absorption by the ground state $CsCl(^1\Sigma)$ molecules. For a concentration increase in the range from about 0.4 up to 0.9% the optimal values of the dopant content correspond to the highest band intensities. The AX content larger than 0.9% results in a decrease of the B–X band intensities. Moreover, in that doping region a rapid growth of the intrinsic fluorescence bands originating from aggregates occurs. In the case of CsF the concentration quenching seems to represent the main negative contribution to the emission efficiency of the excimer band. In general, the effect observed most clearly for CsCl is representative for the decay of $(AX)^+$ states of alkalihalides in general. This is supported by the similar concentration dependences of the band intensities observed for CsF and in part for RbF, too [17,18].

4. Conclusion

The favorable population of the $A^{2+}X^-$ state of alkalihalides by ionization of the trapped AX molecules via host excitons of solid Ne and Ar can be deduced from the energy level scheme and is confirmed experimentally. The $B(^2\Sigma_{1/2})$–$X(^2\Sigma_{1/2})$ radiative transition from ionic states represents the most efficient depopulation channel for *e*-beam excited, rare gas matrix-isolated CsF, CsCl and RbF. Also the much weaker emission bands $C(^2\Pi)$–$A(^2\Pi)$ of $Cs^{2+}F^-$ and $Cs^{2+}Cl^-$ occur besides the intrinsic luminescence bands of aggregates. For RbF and CsCl the concentration dependent formation of X_2^* molecules due to predissociation in the $A^{2+}X^-(B^2\Sigma_{1/2})$ state is observed in experiment. The resulting molecular transition $D'(^3\Pi_{2g})$–$A'(^3\Pi_{2u})$ competes efficiently with the exciplex emissions at low doping concentrations around 0.1%. A strong dependence of the emission intensities on the alkalihalide content leads to aggrega-

tion and quenching at doping concentrations higher than the optimal range of about 0.7 %. Marked difference in the B–X emissions intensities observed for alkalihalides CsF, CsCl and RbF is explained by the position of the crossing point of the $A^{2+}X^{-}$ and $A^{+}X^{*}$ potential surfaces relative to the equilibrium internuclear separation of the $A^{+}X^{-}$ ground state. The condensed phase ionic excimer $Cs^{2+}F^{-}$ represents the best emission properties compared to $Cs^{2+}Cl^{-}$ and $Rb^{2+}F^{-}$. This is demonstrated by the B–X fluorescent transition dominating the excited state decay and also the fluorescence intensity exceeding those of $Cs^{2+}Cl^{-}$ and $Rb^{2+}F^{-}$ by a factor of about 6 and 20, respectively.

1. R. Sauerbrey and H. Langhoff, *IEEE J.* ***QE-21***, 179 (1985).
2. N.G. Basov, M.G. Voitik, V.S. Zuev, and V.P. Kutalchov, *Sov. J. Quantum Electron* **15**, 1455 (1985).
3. H.M.I. Bastiaens, F.T.J.L. Lankhorst, P.J.M. Peters, and W.J. Witteman, *Appl. Phys. Lett.* **60**, 2834 (1992).
4. S. Kubodera, P.J. Wisoff, and R. Sauerbrey, *J. Opt. Soc. Am.* **B9**, 10 (1992).
5. C. Toth, J.F. Young, and R. Sauerbrey, *Opt. Lett.* **18**, 2120 (1993).
6. T.T. Yang, V.T. Gylys, and D.G. Harris, *J. Opt. Soc. Am.* **B6**, 1536 (1989).
7. D. Xing, K. Ueda, and H. Takuma, *Chem. Phys. Lett.* **163**, 193 (1989).
8. S. Kubodera, P.J. Wisoff, and R. Sauerbrey, *J. Chem. Phys.* **92**, 5867 (1990).
9. S. Kubodera and R. Sauerbrey, *Opt. Comm.* **94**, 515 (1992).
10. M. Schumann and H. Langhoff, *J. Chem. Phys.* **101**, 4769 (1994)
11. G. Śliwiński, Ch. Bressler, and N. Schwentner, *Phys. Status Solidi* **B193**, 247 (1996).
12. G. Śliwiński and N. Schwentner, *J. Appl. Phys.* **D30**, 2229 (1997).
13. G. Śliwiński and N. Schwentner, *J. Low Temp. Phys.* **111**, 733 (1998).
14. E.S. Rittner, *J. Chem. Phys.* **19**, 1030 (1951).
15. G. Zerza, G. Śliwiński, and N. Schwentner, *Appl. Phys.* **B55**, 331 (1992)
16. G. Zerza, G. Śliwiński, and N. Schwentner, *Appl. Phys.* **A56**, 156 (1993)
17. M. Frankowski, G. Śliwiński, and N. Schwentner, *SPIE Proc.* **3724**, 362 (1999).
18. M. Frankowski, G. Śliwiński, and N. Schwentner, *J. Low Temp. Phys.* **122**, 443 (2001).